Split-Type Input-Reflectionless Multiband Filters

Roberto Gómez-García, *Senior Member, IEEE*, José-María Muñoz-Ferreras, *Member, IEEE*, and Dimitra Psychogiou, *Member, IEEE*

***Abstract*— Split-type multiband bandpass filters (BPFs) and bandstop filters (BSFs) with input-reflectionless capabilities are reported in this letter. In the multiband BPF case, they consist of a duplexing network with a split-type multiband BPF channel—main channel—and its complementary resistively terminated multiband BSF channel—auxiliary channel—that absorbs the input-signal energy that is not transmitted by the overall filter. The multiband BSF counterpart is obtained from the latter by interchanging the roles of the main and auxiliary channels. The operational foundations, theoretical design rules, and synthesis examples of the devised split-type input-reflectionless multiband filters under a coupling-matrix-based formulation are described. Furthermore, for practical validation purposes, two microstrip prototypes corresponding to 3.85-/4.55-GHz second-order dual-band BPF and BSF circuits are constructed and measured.**

***Index Terms*— 5G circuit, absorptive filter, bandpass filter (BPF), bandstop filter (BSF), dual-band filter, microstrip filter, multiband filter, planar filter, reflectionless filter, split-type filter.**

I. Introduction

SPLIT-TYPE multiband bandpass filters (BPFs) are a suitable alternative as signal-separation devices in multiband RF systems with closely spaced bands. In these filters, the multipassband response is realized by creating rejected bands within a main wider transmission band. This is done by coupling sets of resonators—$N-1$ each for an N-band BPF—to those that determine the main broad passband to divide it into several subbands [1]–[4]. Other applications of this principle are the design of broadband BPFs with in-band tunable notches when the embedded stopbands are spectrally narrow and agile [5]. This research topic related to the development of multiband bandstop filters (BSFs) for multi-interference suppression is gaining interest [6]–[8].

To the best of our knowledge, previously reported split-type multiband BPFs have a reflective-type filtering nature. This means that the RF-input-signal energy that is not transmitted within their stopband regions is reflected back to the source at the input port. However, such unwanted RF-power returns may deteriorate the operation of prior adjacent active stages in a complete RF chain. For example, they may lead to the generation of additional mixing terms in frequency converters or to instability issues in power amplifiers [9]. Whereas interstage isolators or attenuators are commonly used to avoid this problem at the expense of increased circuit size and higher insertion loss, the employment of absorptive or reflectionless filters could be a preferred solution. Nevertheless, available approaches for this kind of filters mainly focus on single-band designs (see [10], [11], [13]) except for basic in-series cascades of separate reflectionless BSF units for multiband BSFs.

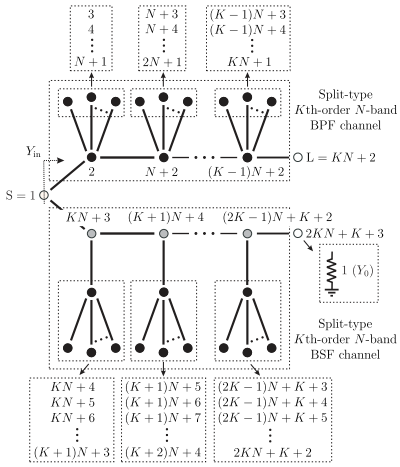

Fig. 1. Normalized coupling-routing diagram of the split-type input-reflectionless Kth-order N-band BPF ($K \geq 1$ and $N \geq 2$)—its BSF version is obtained by interchanging the roles of nodes $KN+2$ and $2KN+K+3$—[black circles: resonating nodes; gray circles: zero-susceptance nonresonating nodes; white circles: unitary source (S), load (L), and loading resistor; continuous lines: couplings; $Y_0 = 1/Z_0$: reference admittance for normalization; Y_{in}: normalized input admittance; and Ω: normalized frequency].

In this letter, a class of split-type multiband BPFs and BSFs with reflectionless behavior at their input terminal is proposed for the first time. They are based on the extrapolation of the input-reflectionless single-band BPF and BSF principles described in [12] to this type of filters. Furthermore, design guidelines from a coupling-matrix perspective and synthesis examples for different number of bands and order are shown.

The rest of this letter is organized as follows. The theoretical operational and design principles for the proposed split-type input-reflectionless multiband BPF and BSF concepts are described in Section II. Section III reports on experimental microstrip prototypes that exhibit second-order dual-band BPF and BSF responses with operational bands allocated within the first Federal Communications Commission (FCC) 5G band (3.5–6 GHz). Finally, summary and main conclusions of this letter are given in Section IV.

II. Theoretical Foundations

The normalized coupling-matrix diagram of the engineered split-type input-reflectionless multiband BPF—Kth-order N-band realization—is shown in Fig. 1. It is composed of a split-type multiband BPF channel—main channel—connected to the overall output port and its complementary (i.e., same-order and opposite transmission frequency profile) multiband BSF channel—auxiliary channel—terminated in a

Manuscript received April 12, 2018; revised August 10, 2018; accepted August 28, 2018. Date of publication September 18, 2018; date of current version November 6, 2018. This work was supported in part by the Spanish Ministry of Economy and Competitiveness under Project TEC2017-82398-R and in part by the National Science Foundation under Award 1731956. *(Corresponding author: Roberto Gómez-García.)*

R. Gómez-García and J.-M. Muñoz-Ferreras are with the Department of Signal Theory and Communications, University of Alcalá, 28871 Alcalá de Henares, Spain (e-mail: roberto.gomez.garcia@ieee.org; jm.munoz@uah.es).

D. Psychogiou is with the Department of Electrical, Computer, and Energy Engineering, University of Colorado Boulder, Boulder, CO 80309 USA (e-mail: dimitra.psychogiou@colorado.edu).

Color versions of one or more of the figures in this paper are available online at http://ieeexplore.ieee.org.

Digital Object Identifier 10.1109/LMWC.2018.2868091

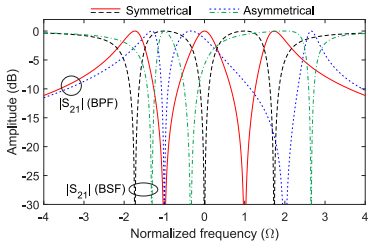

Fig. 2. Theoretical power transmission ($|S_{21}|$) parameter of ideally synthesized symmetrical/asymmetrical first-order triple-band (i.e., $K = 1$ and $N = 3$) examples for the split-type input-reflectionless multiband BPF and BSF architecture in Fig. 1 (symmetrical: $K_{D1} = 1$, $K_{D2} = 1$, and $\Omega_{z2} = 1$; and asymmetrical: $K_{D1} = 0.5$, $K_{D2} = 1.3$, and $\Omega_{z2} = 2$; $K_A = 1$, $K_B = 1$, $\Omega_0 = 0$, and $\Omega_{z1} = -1$ for both examples).

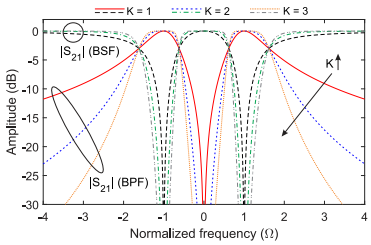

Fig. 3. Theoretical power transmission ($|S_{21}|$) response of ideally synthesized first-, second-, and third-order dual-band (i.e., $K = 1$–3 and $N = 2$) examples for the split-type input-reflectionless multiband BPF and BSF architecture in Fig. 1 ($K = 1$: $K_A = 1$, $K_B = 1$, and $K_{D1} = 1$; $K = 2$: $M_{1,2} = 1/\sqrt{\sqrt{2}}$, $M_{1,7} = 1$, $K_{D1} = 1$, $M_{2,4} = 1$, $M_{4,6} = \sqrt{\sqrt{2}}$, $M_{7,8} = \sqrt{\sqrt{2}}$, $M_{7,10} = 1$, $M_{10,11} = 1/\sqrt{\sqrt{2}}$, and $M_{10,13} = 1$; $K = 3$: $M_{1,2} = \sqrt{2/3}$, $M_{1,9} = 1$, $K_{D1} = 1$, $M_{2,4} = 1/\sqrt{2}$, $M_{4,6} = \sqrt{3/2}$, $M_{6,8} = \sqrt{2}$, $M_{9,10} = \sqrt{3/2}$, $M_{9,12} = 1$, $M_{12,13} = 2/\sqrt{3}$, $M_{12,15} = 1$, $M_{15,16} = 1/\sqrt{2}$, and $M_{15,18} = 1$; and $\Omega_0 = 0$ and $\Omega_{z1} = 0$ for all examples).

reference-impedance resistor. This resistor dissipates the input-signal energy that is not transmitted by the overall filter in its stopband regions so that a perfect input-reflectionless behavior is obtained—i.e., $Y_{\text{in}}(\Omega) = 1\ \forall\Omega$. Note that its split-type multiband BSF counterpart can be realized by interchanging the roles of the multiband BPF and BSF channels.

In the multiband BPF scheme in Fig. 1, the following conditions are imposed for a multipassband transfer function centered at Ω_0 with normalized interpassband transmission-zero frequencies—i.e., normalized interstopband reflection-zero frequencies in the Ω_0-centered multistopband response for the multiband BSF version—at $\Omega_{z1} < \Omega_{z2} < \cdots < \Omega_{z(N-1)}$:

$$M_{(k-1)N+2,(k-1)N+2} = M_{(K+k-1)N+k+3,(K+k-1)N+k+3} = -\Omega_0 \tag{1}$$

$$M_{(k-1)N+n+2,(k-1)N+n+2} = M_{(K+k-1)N+n+k+3,(K+k-1)N+n+k+3} = -\Omega_{zn} \tag{2}$$

$$M^2_{(k-1)N+2,(k-1)N+n+2} = M^2_{(K+k-1)N+k+3,(K+k-1)N+n+k+3} \triangleq K^2_{Dn} \qquad k = 1, 2, \ldots, K, \quad n = 1, 2, \ldots, N-1 \tag{3}$$

$\{M_{i,j}\}$ $(i, j = 1, 2, \ldots, 2KN + K + 3)$ being the coupling-matrix coefficients. Moreover, depending on the intended filter order, the following considerations must be taken into account.

- For first-order designs—i.e., $K = 1$—by imposing the condition $Y_{\text{in}}(\Omega) = 1\ \forall\Omega$ [12], the following design relationships along with (1)–(3) to be satisfied to attain a perfect input-reflectionless behavior are obtained:

$$M^2_{1,2} = M^2_{2,N+2} \triangleq K^2_A \tag{4}$$

$$M^2_{1,N+3} = M^2_{N+3,2N+4} \triangleq K^2_B \tag{5}$$

$$M^2_{N+3,N+4} \triangleq K^2_C = K^2_A K^2_B. \tag{6}$$

  For illustration purposes, the power transmission response of theoretical first-order triple-band BPF and BSF examples synthesized through (1)–(6) is depicted in Fig. 2. As proven, symmetrical and asymmetrical transfer functions with arbitrary characteristics in terms of frequency spacing between bands and their bandwidths can be realized by properly adjusting the design variables after imposing the input-reflectionless conditions—i.e., K_A, K_{D1}, K_{D2}, Ω_0, Ω_{z1}, and Ω_{z2} in this case.
- For higher order designs—i.e., $K \geq 2$—the derivation of analytical formulas for the coupling-matrix coefficients becomes more tedious. However, optimization procedures can be used for their computation depending on the prefixed transfer-function specifications. Fig. 3 shows the power transmission response of theoretical first-, second-, and third-order dual-band BPF and BSF examples with the same 3-dB bandwidths, in which the selectivity increase for higher filter orders while preserving the fully input-reflectionless behavior can be appreciated.

Note also that, as in [13], for single-band BSFs, split-type multiband filters with reflectionless behavior at both ports are feasible by using a resistively terminated branch at both filter accesses. However, this is done at the expense of higher number of circuit elements and design complexity and passing from a fully reflectionless behavior to a quasi-absorptive one.

III. Experimental Results

To prove the practical viability of the proposed split-type input-reflectionless multiband BPF and BSF principles, 50-Ω-referred 3.85-/4.55-GHz second-order dual-band BPF and BSF prototypes have been manufactured in microstrip technology and measured (i.e., $Z_0 = 50\ \Omega$ and $f_0 = f_{z1} = 4.2$ GHz). The dual-band BPF circuit exhibits 3-dB absolute bandwidths for the two bands of 350 MHz (i.e., equal to 9.1% and 7.7% in relative terms for the lower and upper bands, respectively), whereas the other prototype consists of its BSF counterpart.

In these designs, the resonators were realized as open-ended half-wavelength-at-4.2-GHz transmission-line segments with $0.7Z_0$ characteristic impedance and the impedance inverters as quarter-wavelength transmission-line ones. The power transmission and input-reflection parameters of the theoretically synthesized input-reflectionless dual-band BPF and BSF—i.e., case $Z_R = Z_{R1} = 0.7Z_0$—are depicted in Fig. 4. As can be seen, a 10-dB-referred input-power-matching range of 2.52–5.88 GHz—i.e., 2.33:1 ratio—is obtained. Note that the resulting responses for $Z_R = 1.7Z_0$ and $Z_{R1} = 0.3Z_0$ are also included to show how the operational bandwidths can be adjusted through them for fixed impedance inverter values.

The photographs of the developed microstrip dual-band filter prototypes are given in Fig. 5. Their simulated—by means of the commercial package Ansys HFSS—and measured—with an Agilent-E8361A network analyzer—power-transmission, input-reflection, and measured output-reflection responses are depicted in Fig. 6. As shown, a fairly close agreement between simulations and measurements

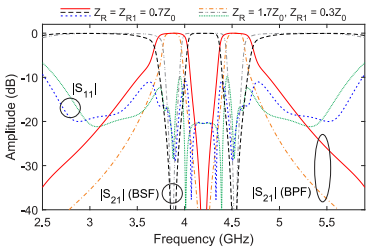

Fig. 4. Power transmission ($|S_{21}|$) and input-reflection ($|S_{11}|$) responses of the theoretically synthesized split-type input-reflectionless second-order dual-band BPF and BSF: bandwidth adjustment through the characteristic impedances Z_R and Z_{R1} of the f_0 and f_{z1} resonators ($Z_{1,2} = 1.4Z_0$, $Z_{1,7} = 1.1Z_0$, $Z_{D1} = 2.2Z_0$, $Z_{2,4} = 2Z_0$, $Z_{4,6} = 1.4Z_0$, $Z_{7,8} = 1.1Z_0$, $Z_{7,10} = Z_0$, $Z_{10,11} = 1.1Z_0$, and $Z_{10,13} = Z_0$ for both examples, where the subindex notation in Fig. 1 for $K = 2$ and $N = 2$ has been used).

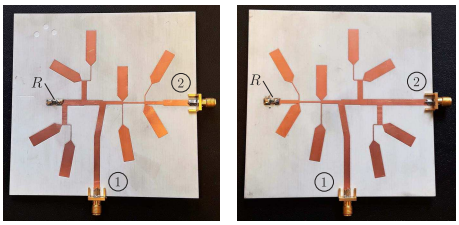

(a) (b)

Fig. 5. Photographs of the manufactured microstrip split-type input-reflectionless dual-band filter prototypes (Rogers 4003C substrate: relative dielectric permittivity $\varepsilon_r = 3.38$, dielectric thickness $H = 1.524$ mm, metal thickness $t = 17.8$ μm, and dielectric loss tangent $\tan(\delta_D) = 0.0027$; ground connections for 50-Ω loading resistors: 1-mm-diameter metallic via holes). (a) Dual-band BPF. (b) Dual-band BSF (occupied area for both circuits: 8.25×8.41 cm^2).

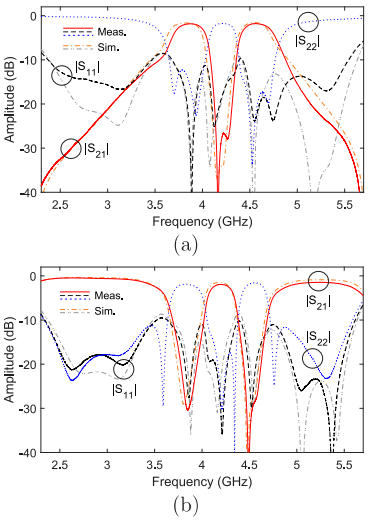

(a)

(b)

Fig. 6. Simulated and measured power transmission ($|S_{21}|$), input-reflection ($|S_{11}|$), and measured output-reflection ($|S_{22}|$) responses of the manufactured microstrip split-type input-reflectionless dual-band filter prototypes. (a) Dual-band BPF. (b) Dual-band BSF.

is obtained. The main measured characteristics of the dual-band BPF are as follows: lower and upper passbands with center frequencies of 3.86 and 4.58 GHz, 3-dB absolute bandwidths of 359 and 369 MHz—i.e., equal to 9.3% and 8.1% in relative terms—minimum in-band insertion-loss levels of 1.8 dB—for both passbands—minimum in-band power-matching levels of 10.1 dB and 9.7 dB, and lower and upper 10-dB input-power-matching frequencies of 2.37 and 5.54 GHz—i.e., 2.34:1 ratio. The dual-band BSF exhibits measured lower and upper stopbands with rejection depths of 30.4 and 61 dB at 3.85 and 4.5 GHz, respectively, 3-dB absolute bandwidths of 488 and 421 MHz—i.e., of 12.7% and 9.4% in relative terms—minimum in-band input-power-matching levels of 9.5 and 10.2 dB, lower and upper 10-dB input-power-matching frequencies of 2.34 and 5.62 GHz—i.e., 2.4:1 ratio—and minimum power-insertion loss levels in the lower, middle, and upper passband ranges of 0.5, 1.9, and 1.5 dB.

IV. Conclusion

Split-type input-reflectionless multiband BPFs and BSFs based on a complementary duplexer approach have been proposed for the first time. A coupling-matrix-based formulation for these filters and guidelines for their theoretical design supported by various synthesis examples have been provided. Moreover, for experimental-verification purposes, second-order dual-band BPF and BSF microstrip prototypes with operational bands allocated within the first FCC 5G band (3.5–6 GHz) have been developed and characterized.

References

[1] A. Garcia-Lamperez and M. Salazar-Palma, "Single-band to multiband frequency transformation for multiband filters," *IEEE Trans. Microw. Theory Techn.*, vol. 59, no. 12, pp. 3048–3058, Dec. 2011.

[2] S. Zhang and L. Zhu, "Compact split-type dual-band bandpass filter based on $\lambda/4$ resonators," *IEEE Microw. Wireless Compon. Lett.*, vol. 23, no. 7, pp. 344–346, Jul. 2013.

[3] C. Zhu, J. Xu, G. Zhang, W. Kang, and W. Wu, "Split-type dual-band bandpass filters with symmetric/asymmetric response," *IEEE Microw. Wireless Compon. Lett.*, vol. 28, no. 1, pp. 25–27, Jan. 2018.

[4] P. Ma *et al.*, "A design method of multimode multiband bandpass filters," *IEEE Trans. Microw. Theory Techn.*, *IEEE Trans. Microw. Theory Techn.*, vol. 66, no. 6, pp. 2791–2799, Jun. 2018.

[5] D. Psychogiou, R. Gómez-García, and D. Peroulis, "Fully adaptive multiband bandstop filtering sections and their application to multifunctional components," *IEEE Trans. Microw. Theory Techn.*, vol. 64, no. 12, pp. 4405–4418, Dec. 2016.

[6] X. Luo, J.-G. Ma, K. S. Yeo, and E.-P. Lin, "Compact ultra-wideband (UWB) bandpass filter with ultra-narrow dual- and quad-notched bands," *IEEE Trans. Microw. Theory Techn.*, vol. 59, no. 6, pp. 1509–1519, Jun. 2011.

[7] W. J. Feng, M. L. Hong, W. Q. Che, and Q. Xue, "Dual-band microstrip bandstop filter with multiple transmission poles using coupled lines," *IEEE Microw. Wireless Compon. Lett.*, vol. 27, no. 3, pp. 236–238, Mar. 2017.

[8] D. Psychogiou, R. Gómez-García, and D. Peroulis, "Wide-passband filters with in-band tunable notches for agile multi-interference suppression in broad-band antenna systems," in *Proc. IEEE Radio Wireless Symp.*, Anaheim, CA, USA, Jan. 2018, pp. 213–216.

[9] Mini-Circuits, Brooklyn, N.Y., "Reflectionless filters improve linearity and dynamic range, " *Microw. J.*, vol. 58, no. 8, pp. 42–50, Aug. 2015.

[10] A. C. Guyette, I. C. Hunter, and R. D. Pollard, "Design of absorptive microwave filters using allpass networks in a parallel-cascade configuration," in *IEEE MTT-S Int. Microw. Symp. Dig.*, Boston, MA, USA, Jun. 2009, pp. 733–736.

[11] M. A. Morgan and T. A. Boyd, "Theoretical and experimental study of a new class of reflectionless filter," *IEEE Trans. Microw. Theory Techn.*, vol. 59, no. 5, pp. 1214–1221, May 2011.

[12] D. Psychogiou and R. Gómez-García, "Reflectionless adaptive RF filters: Bandpass, bandstop, and cascade designs," *IEEE Trans. Microw. Theory Techn.*, vol. 65, no. 11, pp. 4593–4605, Nov. 2017.

[13] R. Gómez-García, J.-M. Muñoz-Ferreras, and D. Psychogiou, "Symmetrical quasi-reflectionless BSFs," *IEEE Microw. Wireless Compon. Lett.*, vol. 28, no. 4, pp. 302–304, Apr. 2018.